On the Oscillatory Solutions in Hyperbolic Conservation Laws

George R. Peters *
Department of Mathematics
Iowa State University
Ames, IA 50011

Sunčica Čanić †
Department of Mathematics
Iowa State University
Ames, IA 50011

Abstract. In this paper we investigate solutions of hyperbolic Riemann problems that arise in situations when weak self-similar solutions consisting of constant states, rarefaction waves and/or jump discontinuities that satisfy the viscous profile entropy criterion, do not exist. We concentrate on two models: the shallow water equations and on a three-phase flow model derived from petroleum engineering. For these two models we consider hyperbolic Riemann initial data that correspond to Lax shocks that do not admit viscous profiles due to the presence of limit cycles in the dynamical system associated with the admissibility criterion.

We show that in these two models, solutions exhibiting continuously generated oscillations take place and satisfy the inviscid system of conservation laws in a measure-valued sense.

To show the main result of this work we study Riemann solutions of inviscid systems of conservation laws obtained in the singular limit of the associated parabolic systems. We solve the parabolic problems numerically and prove that the inviscid limit of numerical solutions of the parabolic problems is a measure-valued solution of the hyperbolic conservation law.

Key words. Conservation laws, oscillatory solutions, measure-valued solution, viscous profile entropy criterion

AMS subject classification. 35L65, 35L67, 58F14, 76S05, 76T05;

1 Introduction

In this paper we investigate solutions of Riemann problems that arise in situations when weak self-similar solutions consisting of constant states, rarefaction waves and/or jump discontinuities (shock waves) do not exist. We adopt the viscous profile entropy criterion to distinguish physically admissible shock waves. We concentrate on two models: the shallow water equations and on a quadratic model

* This work was supported in part by the National Science Foundation graduate student summer support as part of grant DMS-9626831. Present address: Department of Mathematics, University of Houston, Houston TX 77204. E-mail address: canic@math.uh.edu.

† This work was supported by the National Science Foundation, grant DMS-9626831, and in part by the Department of Energy grant DE-FG02-94ER25220

derived from petroleum engineering. The results of Refs. [5] and [3] show that for certain viscosity matrices, the viscous profile entropy criterion is too selective in reducing the number of solutions to guarantee existence of weak self-similar solutions. In fact, in Ref. [5] it was shown that, for the shallow water equations, nonexistence occurs for a "generic" symmetric positive definite viscosity matrix and an open set of Riemann initial data. The focus of the current paper is on the study of solutions that take place when those weak self-similar solutions do not exist. As in Refs. [5] and [3] we consider cases in which nonexistence is due to the presence of a limit cycle in the dynamical system associated to the viscous profile entropy criterion. We study solutions of the inviscid problem by taking the singular limit of solutions of the associated parabolic problems. We show that in both models, solutions exhibiting continuously generated oscillations take place. The oscillations stay uniformly bounded but increase in frequency as viscosity parameters approach zero. We prove that in the inviscid limit the oscillatory solutions define a measure-valued solution of the conservation law, as studied by DiPerna and Tartar in [9, 27].

The "oscillatory irregularity" presented in this paper is not isolated to the two initial value problems considered here. We observed this behavior for an open set of viscosity parameters, and for an open set of initial data in both models. Furthermore, since the shallow water equations are equivalent to the isentropic equations of gas dynamics with $\gamma = 2$, we expect this behavior to occur in gas dynamics with certain viscosity parameters, as well. Oscillatory behavior has also been discussed in a vast literature related to phase transitions, in particular, the formation of a band-like structure in a crystal of memory alloy during austenitic-martensitic transformation. In the form of a conservation law, oscillatory solutions for phase transitions were studied in Ref. [14]. Furthermore, the work of DiPerna and Majda [10] reports on oscillations and concentrations arising in incompressible flow, as well. Oscillations inside the elliptic region for a problem of mixed type were studied in Ref. [13], and an initial-boundary value problem for multiphase flow equations giving rise to oscillations (but with diffusion matrix equal to a multiple of the identity) was studied in Ref. [12].

In addition to the study of oscillatory solutions, in this paper we also establish a relationship between the oscillatory solutions, described above, and L^2 linearized instability studied by Majda and Pego [22]. More specifically, in Ref. [22] Majda and Pego define stable viscosity matrices $D(U)$ by requiring that for every state U the Cauchy problem for the associated linearized parabolic problem is uniformly well posed in L^2, as the parameter ϵ that multiplies the viscosity, approaches zero. In Ref. [6] Čanić and Plohr viewed this condition as a condition on a state U being stable or not in the sense of Majda and Pego. Results of Ref. [5] show that for a "generic", positive definite viscosity matrix there is an open region of hyperbolic states consisting of points that are unstable for the shallow water equations. Riemann initial data for which at least one of the states lies in the unstable region lead to nonexistence of Riemann solutions [5]. For both models, the shallow water equation and the three-phase flow model, we consider single shock initial data that falls in the class considered in [5] and is unstable in the sense of Majda and Pego, and show that measure-valued solutions take place. The expectation values of the measure-valued solutions consist of shocks that satisfy the following form of the Rankine-Hugoniot condition

$$-s\left[\overline{U}-\overline{U}_{-}\right]+\overline{F}(U)-\overline{F}(U_{-})=0,$$

where $\overline{U}$ and $\overline{F}$ are the expectation values, with respect to the underlying Young measure, of the state variable and the flux function, respectively. Furthermore, to emphasize the fact that unstable initial data arise in realistic models, we show that there is a nontrivial Majda-Pego unstable region for a three-phase flow model arising in oil recovery and a particular viscosity matrix deriving from capillary pressures (Appendix A).

In this paper we do not offer answers to the question about the physical meaning of the oscillations. We believe that the answer depends on the model at hand. We speculate that in the three-phase flow equations the oscillations describe interspersing of different phases. If this is indeed the case we will have to live with this radically different notion of solution than what is normally expected. Otherwise, we will need to redefine the equations. One idea would be to, for example, introduce a "renormalized" flux function F_{ren} such that $F_{ren}(\overline{U}) = \overline{F}(U)$ to obtain a closed system of equations (see Remark 4 in Section 4.3). This could be done, for example, in the spirit of the convexified Maxwell construction to redefine the problem in a (possibly) physically correct manner.

1.1 Background

We consider systems of conservation laws in one space dimension

$$U_t + F(U)_x = 0, \quad x \in \mathbf{R}, \quad t > 0, \tag{1}$$

where the state variable U lies in the state space $\mathcal{U} \subseteq \mathbf{R}^2$, and the flux $F : \mathcal{U} \to \mathbf{R}^2$ is continuously differentiable. In particular, we consider the above systems with Riemann initial conditions,

$$U(x,0) = \begin{cases} U_L, & x < 0 \\ U_R, & x > 0 \end{cases}. \tag{2}$$

We assume that our initial data lies in the strictly hyperbolic region of state space, namely, in the region consisting of points U for which the Jacobian $F'(U)$ has distinct real eigenvalues. Moreover, in this paper we study Riemann problems with *shock initial data*, *i.e.*, initial data (2) that satisfy the Rankine-Hugoniot condition

$$s(U_+ - U_-) = F(U_+) - F(U_-)$$

and the Lax characteristic inequalities [19]

$$\lambda_i(U_-) > s > \lambda_k(U_+) \text{ and } \operatorname{sgn}(\lambda_j(U_-) - s) = \operatorname{sgn}(\lambda_j(U_+) - s) \neq 0, \quad \text{for } i \neq j.$$

However, the entropy criterion used in this paper is *not* the Lax characteristic entropy criterion. We consider a shock wave *admissible* if it satisfies the *viscous profile entropy criterion.* Namely, following Gel'fand [16], we study an associated viscous regularization

$$U_t + F(U)_x = \epsilon(D(U)U_x)_x, \tag{3}$$

with $D(U) = D$ corresponding to a constant viscosity (diffusion) matrix satisfying the *strict parabolicity condition* $\mathrm{Re}(d_i) > 0$ for each eigenvalue d_1, d_2 of D. A shock between U_- and U_+ traveling with speed s, (U_-, U_+, s), is considered admissible if it can be obtained in the limit, as $\epsilon \to 0$, of traveling wave solutions $\widetilde{U}(\xi) = \widetilde{U}((x - st)/\epsilon)$ of the parabolic system (3) with the asymptotic states $\lim_{\xi\to\pm} \widetilde{U} = U_\pm$. Such a traveling wave corresponds to a connecting orbit in the dynamical system

$$U' = D^{-1}[-s(U - U_-) + F(U) - F(U_-)] \tag{4}$$

between the critical points U_- and U_+, traversed in the direction from U_- to U_+. A complete list of admissible shock waves that may comprise a weak Riemann solution is the following:

- a compressive repellor→ saddle shock wave, or a 1-shock wave (which corresponds to a connecting orbit from a repellor U_- to a saddle U_+, with the characteristic structure consisting of three converging characteristics and one outgoing characteristic),

- a compressive saddle→ attractor shock wave, or a 2-shock wave (which corresponds to a connecting orbit from a saddle U_- to an attractor U_+, with the characteristic structure consisting of three converging characteristics and one outgoing characteristic),

- a saddle→ saddle shock wave, or a transitional shock wave (which corresponds to a connecting orbit from a saddle U_- to a saddle U_+; thus the characteristic structure consists of two converging and two outgoing characteristics),

- a repellor→attractor shock wave, or an overcompressive shock wave (which corresponds to a connecting orbit from a repellor U_- to an attractor U_+; thus the characteristic structure consists of four converging characteristics).

(For a relationship between the Lax characteristic entropy criterion and the viscous profile entropy criterion see, for example, Refs. [6, 8, 11, 20, 23].)

We note that if D is different from a multiple of the identity, a critical point that is a repellor in the case when $D = I$ may become an attractor for $D \neq I$, and similarly, an attractor for $D = I$ may become a repellor for $D \neq I$. (Since D is positive definite, saddle points for $D = I$ stay saddle points for $D \neq I$.) One consequence of this property is that there are repellor to saddle shock waves and saddle to attractor shock waves whose characteristic structure consists of three outgoing and one incoming characteristic. These expansive or rarefaction-shock waves have been studied in Ref. [8]. Their presence is tied with the existence of a nontrivial "Majda-Pego region of linearized instability". Namely, in Ref. [22] Majda and Pego studied *stable viscosity matrices* D(U) and showed that for a 2×2 system the stable viscosity matrix criterion

$$l_j(U)D(U)r_j(U) \geq 0, \quad j = 1, 2$$

is equivalent to the linearized bounded L^2 stability of a constant state U. Here $l_j(U)$ and $r_j(U)$ are the left and the right eigenvectors of $F'(U)$. As mentioned in the introduction, in Ref. [6] this condition is viewed as a condition on a state U being stable or not in the sense of Majda-Pego. Moreover, in Ref. [6] the boundary of the region containing stable states has been associated with the presence of the Bogdanov-Takens bifurcation in the dynamical system (4). We call this boundary the *Majda-Pego boundary*. We will see in Section 2 and in Appendix A that realistic models arising in petroleum engineering contain nontrivial regions of hyperbolic states that are *unstable* in the sense of Majda and Pego. Based on the long term stability considerations we disregard expansive shock waves. This is because expansive shock waves were shown to be unstable under small perturbations as solutions of the parabolic PDE (3). See Ref. [28]. This is because the Majda-Pego instability occurs in the outgoing characteristic field and thus can never get swallowed by the shock.

In this paper we study Riemann problems with shock initial data that does not possess a viscous profile due to the presence of a limit cycle surrounding one of the critical points U_L or U_R in the dynamical system (4). In Ref. [5] such initial data was obtained by studying the universal unfolding of the Bogdanov-Takens bifurcation that takes place at the boundary of the unstable Majda-Pego region. Such an initial shock is not a solution of the Riemann problem because it does not comply with the viscous profile entropy criterion. The question is whether there are other waves that can be used to construct a weak self-similar solution? For both models studied in this work, Refs. [5] and [3] imply that this is not the case. More precisely, Refs.[5] and [3] imply that it is not possible to construct a weak self-similar solution consisting of constant states separated by rarefaction waves and/or jump discontinuities that satisfy the viscous profile entropy criterion. Here by a weak solution we mean a bounded measurable function $U(x,t)$ such that

$$\int_0^\infty \int_{-\infty}^\infty U\phi_t + F(U)\phi_x dxdt + \int_{-\infty}^\infty U(x,0)\phi(x,0)dx = 0, \tag{5}$$

for all $\phi(x,t) \in C_0^\infty$. To investigate what type of a solution exists in those situations we study solutions of the parabolic equation (3) in the limit as $\epsilon \to 0$, with the shock initial data (U_L, U_R). To interpret the (limiting) solution of the inviscid problem, we need a notion of a measure-valued solution developed in Refs. [9] and [27].

DEFINITION 1 *Let $P(\mathbf{R}^2)$ denote the set of all probability measures of $\mathbf{R}^2$. We say that $\nu : \mathbf{R} \times [0,\infty) \to P(\mathbf{R}^2)$ is a measure-valued solution of the system of conservation laws* (1) *if for all $\phi \in C_0^\infty$*

$$\begin{aligned}\int_0^\infty \int_{-\infty}^\infty \{\langle \nu_{x,t}, U\rangle\, \phi_t + \langle \nu_{x,t}, F(U)\rangle\, \phi_x\}\, dxdt \\ + \int_{-\infty}^\infty U_0(x)\phi(x,0)dx = 0.\end{aligned} \tag{6}$$

Related to this is the following result which we will use in Section 4.

LEMMA 1 *If $U_\ell(x,t)$ is a sequence in $L^\infty(\mathbf{R}\times[0,\infty),\mathbf{R}^2)$, satisfying $U_\ell(x,t) \in K$ almost everywhere, where K is a compact subset of $\mathbf{R}^2$, then there exists a family of probability measures $\nu_{x,t}$ and a subsequence U_{l_k} such that for all $h \in C(\mathbf{R}^2)$*

$$\begin{aligned} h(U_{l_k}(x,t)) \longrightarrow \overline{h}(x,t) &\equiv \langle \nu_{x,t}, h\rangle \\ &\equiv \int_{K\subset\mathbf{R}^2} h(U)d\nu_{x,t}(U) \end{aligned} \tag{7}$$

where $\longrightarrow$ denotes convergence in the weak- topology of L^∞.*

In the next section we summarize the main results.

1.2 OVERVIEW OF THE PAPER

In Section 2 we present a brief discussion of the models we study in this work. For completeness, in Section 3 we summarize the results from Refs. [5] and [3] that establish nonexistence of Riemann solutions for the two Riemann initial-value problems studied here.

Next we investigate the types of solutions that take place when weak self-similar solutions do not exist. We use Crank-Nicholson method as used by Beam and Warming [2] to investigate solutions of the parabolic equation (3) in the limit as $\epsilon \to 0$, with a fixed positive definite viscosity matrix $D(U) = D$. The numerical method is described in Section 4.1. We find that as $\epsilon \to 0$ the solutions exhibit persistent and stable oscillations of the state variables that increase in frequency but stay uniformly bounded as epsilon decreases. We provide evidence that these oscillations are not numerical aberrations but a property of the solutions themselves. Based on numerical evidence of uniform boundedness of the sequence of numerical solutions we show that there exists a subsequence of numerical solutions that converges in the weak-* topology of L^∞ and prove that the limit is a measure-valued solution of the conservation law. We then show that the entire sequence converges to the measure-valued solution.

Numerical results are presented in Section 5. They show that the expectation values $\overline{U}$ and $\overline{F}$ indeed satisfy the hyperbolic system of conservation laws in a measure-valued sense. We do not calculate the Young measures explicitly. Instead, we approximate the expectation values $\langle \nu_{x,t}, U\rangle$ and $\langle \nu_{x,t}, F(U)\rangle$ from Definition 1 using the sequence of numerical solutions that generate the measure. We observe that the expectation values of the solutions consist of shocks traveling with speed s, where each shock satisfies the Rankine-Hugoniot condition for the expectation values $\overline{U}$ and $\overline{F}$

$$-s(\overline{U}_+ - \overline{U}_-) + \overline{F}_+ - \overline{F}_- = 0.$$

Notice that since F is nonlinear, $\overline{F}(U) \neq F(\overline{U})$.

We note that in both examples our Riemann data consists of a single Lax shock that does not admit a viscous profile, whereas the expectation values of the measure-valued solutions consist of at least two shocks, none of which correspond to the initial shock wave.

We believe that the mechanism that is responsible for the existence of oscillatory solutions is the Majda-Pego instability, described in Section 1.1. We base our belief on several experiments that we ran on data that does not lie in the unstable region. In all such cases we were able to recover a "classical weak" Riemann solution consisting of constant states, rarefaction waves, and/or jump discontinuities.

To emphasize the fact that unstable regions in the sense studied by Majda and Pego arise in realistic models, in Appendix A we consider a full set of the three-phase flow equations in terms of the saturation variables without simplifications which give rise to the quadratic model presented in Section 2, and use a diffusion matrix that derives from the capillary pressures. We show that there is a nontrivial subregion of the state space containing hyperbolic points that are unstable in the sense of Majda and Pego.

Finally, in Appendix B we discuss numerical results that are obtained with a different numerical method and different spatial and temporal discretization and show that the oscillations we obtain in these cases are the same as the oscillations obtained with the linearized Crank-Nicholson method and a particular discretization chosen for stability.

2 Models

In this section we describe the two models that we study in this work. They are the shallow water equations and a quadratic model deriving from petroleum engineering.

2.1 Shallow Water Equations

We study the shallow water equations [21]

$$\begin{bmatrix} v \\ \phi \end{bmatrix}_t + \begin{bmatrix} v^2/2 + \phi \\ v\phi \end{bmatrix}_x = \begin{bmatrix} 0 \\ 0 \end{bmatrix} \tag{8}$$

where v is the velocity and ϕ is the depth of water times a constant gravitational acceleration. Denoting

$$U = \begin{bmatrix} v \\ \phi \end{bmatrix} \text{ and } F(U) = \begin{bmatrix} v^2/2 + \phi \\ v\phi \end{bmatrix}, \tag{9}$$

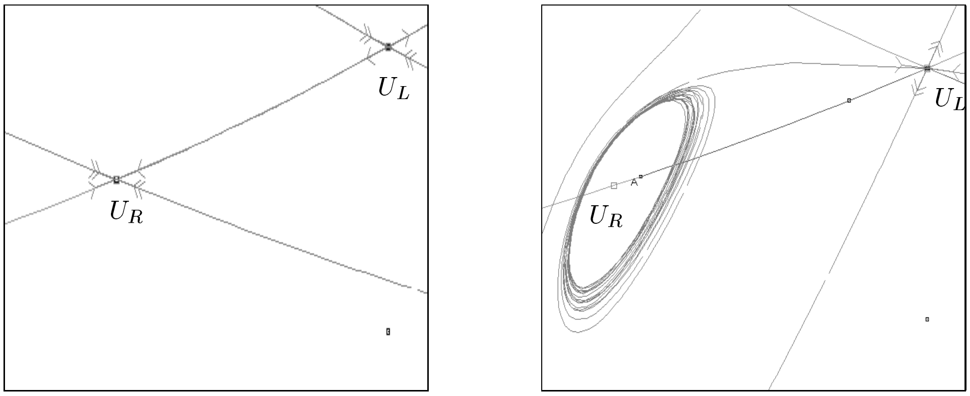

FIGURE 1: Shallow Water Equations: The left picture shows the connecting orbit in the dynamical system with $D = I$. The right picture shows the dynamical system when D is given by (11). The lack of a connecting orbit is due to a limit cycle surrounding the attractor U_R. These Figures were generated with the Riemann problem solver package [17].

we study the Riemann problem for this system with

$$U_L = \begin{bmatrix} 0.00 \\ 0.12 \end{bmatrix} \text{ and } U_R = \begin{bmatrix} -0.1840 \\ 0.0642 \end{bmatrix}. \tag{10}$$

For a viscosity matrix we use the positive definite matrix

$$D = \begin{bmatrix} 13.0116 & -5.9144 \\ -5.9144 & 3.1429 \end{bmatrix}. \tag{11}$$

The U_L, U_R, and D were chosen so that U_L and U_R satisfy the Rankine-Hugoniot condition and the Lax characteristic inequalities that define a Lax 2-shock, but there is not a self-similar Riemann solution between U_L and U_R where the shocks satisfy the viscous profile entropy criterion. Namely, as shown in Ref. [5], U_L and U_R correspond to a saddle and an attractor respectively, in the dynamical system (4), and there is a repelling limit cycle surrounding the critical point U_R which prevents the existence of a connecting orbit from U_L to U_R. See Figure 1. In Ref. [5] it was also shown that there is an open set of initial data that satisfy these properties, and that this type of initial data can be found for every symmetric, nondiagonal, positive definite viscosity matrix. We note that the left and right states lie in the strictly hyperbolic region of state space.

2.2 THREE-PHASE FLOW MODEL

We are concerned with three-phase Buckley-Leverett flow. The three phases are gas, water, and oil. For simplicity we assume that rock porosity, rock permeability, and the mass densities of the three phases, are constant. In addition,

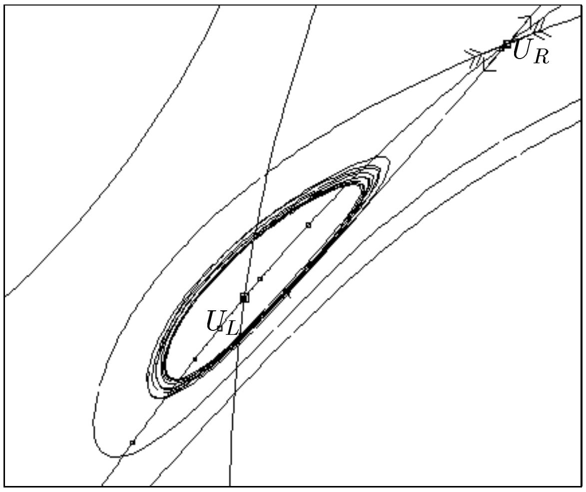

Figure 2: Three-Phase Flow: Attracting limit cycle surrounding the repellor U_L.

we assume that the phase viscosities, are constant. The model consists of two equations describing conservation of mass for each fluid, combined with Darcy's force law. See Ref. [1]. The state variables, s_i, correspond to the saturations of different phases, with $s_3 = 1 - s_2 - s_3$. To further specify the model, we define the relative permeabilities. We study a small perturbation (generalization) of a model proposed by Corey, Pope, and Marchesin, *i.e.*, the model for which the relative permeabilities, κ_i, are given by $\kappa_i = s_i^2, i = 1,2,3$. This gives rise to a conservation law that is strictly hyperbolic everywhere in state space except at a single point, called the umbilic point. To avoid this nongeneric situation we let

$$k_1 = s_1^2 + a_1(c, s_1, s_2), \quad k_2 = s_2^2 + a_2(c, s_1, s_2)$$

be small perturbations of the Corey-Pope-Marchesin relative permeabilities such that the resulting conservation law has a small, nontrivial, elliptic region in state space. Here c measures the size of the elliptic region, and a_1 and a_2 approach zero as $c \to 0$. The functions a_1 and a_2 are selected so that the flux of the resulting system is the same as the flux of the Corey-Pope-Marchesin model plus an appropriate linear term which defines the elliptic region "centered" around the umbilic point. The general form of the coefficients a_1 and a_2 is obtained by Peters in Ref. [24].

To simplify the analysis we consider the quadratic model obtained by the expansion of the flux function about the "center" of the elliptic region. The resulting quadratic model is then put into the normal form (see Refs. [4], [24]) to obtain

$$U_t + F(U)_x = 0, \quad x \in \mathbf{R}, \quad t > 0, \tag{12}$$

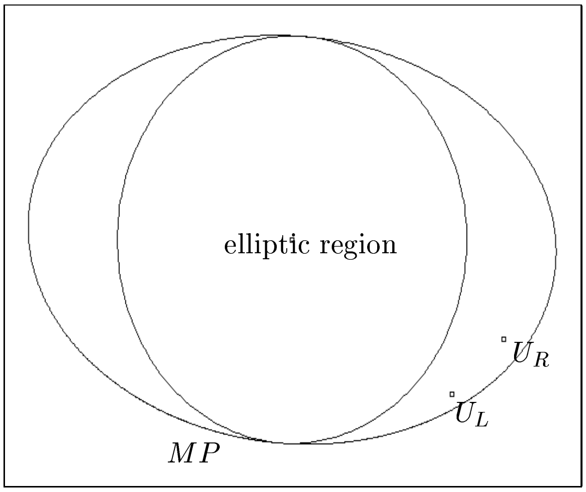

FIGURE 3: Three-Phase Flow: The interior of the outer ellipse contains the points U that are unstable in the sense studied by Majda and Pego. The states U_L and U_R lie in the unstable Majda-Pego region.

with

$$F(U) := \begin{pmatrix} -\frac{1}{2}u^2 + \frac{1}{2}v^2 + cv \\ uv - cu \end{pmatrix}. \tag{13}$$

For $c = 0$ this is a "Case I"-model from Schaeffer-Shearer classification of quadratic models with an umbilic point. See Ref. [25].

In this model, diffusion D can be related to capillary pressures, and is generally different from the identity matrix. See Appendix A. In this work we take the diffusion matrix (or the viscosity matrix) to be a constant, symmetric matrix

$$D = 10^{-3} \begin{pmatrix} 9.7 & -2 \\ -2 & 67.5 \end{pmatrix} \tag{14}$$

that satisfies the *strict parabolicity* condition $\mathrm{Re}(d_i) > 0$ for each eigenvalue d_1, d_2 of D. Indeed, the eigenvalues of D are $d_1 = 0.0096$ and $d_2 = 0.067$. Any small perturbation of a multiple of the identity matrix would give the desired result, however, for numerical purposes it is best if we take D to be a large perturbation of the identity matrix, as given by (14).

We consider shock Riemann data

$$U_L = \begin{pmatrix} 0.211525 \\ -0.17545 \end{pmatrix}, \quad U_R = \begin{pmatrix} 0.279759 \\ -0.113712 \end{pmatrix}, \tag{15}$$

that corresponds to a Lax 1-shock that does not admit a viscous profile due to the presence of an attracting limit cycle in the dynamical system (4) surrounding the repellor U_L. The corresponding phase space portrait is shown in Figure 2.

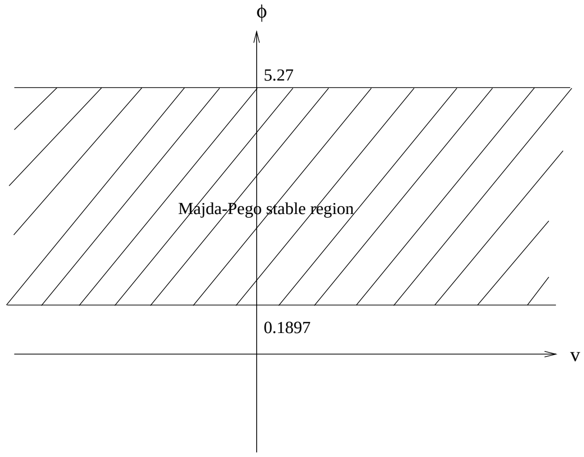

Figure 4: Shallow water equations: Majda-Pego stable region for the viscosity matrix (11) with $a = 13.0116$, $b = 5.9144$ and $c = 3.1429$. The figure shows that the region of stable points lies between $\phi = 0.1897$ and $\phi = 5.27$.

The states U_L and U_R lie in the region of linearly unstable points in the sense of Majda and Pego, as was described in Section 1.1. The relationship between the Majda-Pego region of linearized instability and the left and right states U_L and U_R is shown in Figure 3. The size of the unstable region relative to the entire state space is shown in Figure 13 in Appendix A.

3 Nonexistence of weak solutions

In this section we discuss nonexistence of scale-invariant weak solutions consisting of constant states, rarefaction waves, and/or viscous admissible shock waves, for the two Riemann problems described in the previous section. We first summarize the results from Ref. [5] which establish nonexistence of Riemann solutions for an open set of Riemann initial data and a generic, positive definite, symmetric viscosity matrix, and show that our initial data and the viscosity matrix fall into the class studied in [5]. We then comment on the results of Ref. [3] which establish nonexistence of self-similar weak solutions for the quadratic model deriving from petroleum engineering. The fundamental difference in those two models in showing nonexistence of self-similar solutions lies in the fact that, in contrast to the quadratic model arising from petroleum engineering, the shallow water equations do not admit "nonclassical" shock waves, *i.e.*, transitional (undercompressive) or overcompressive shock waves.

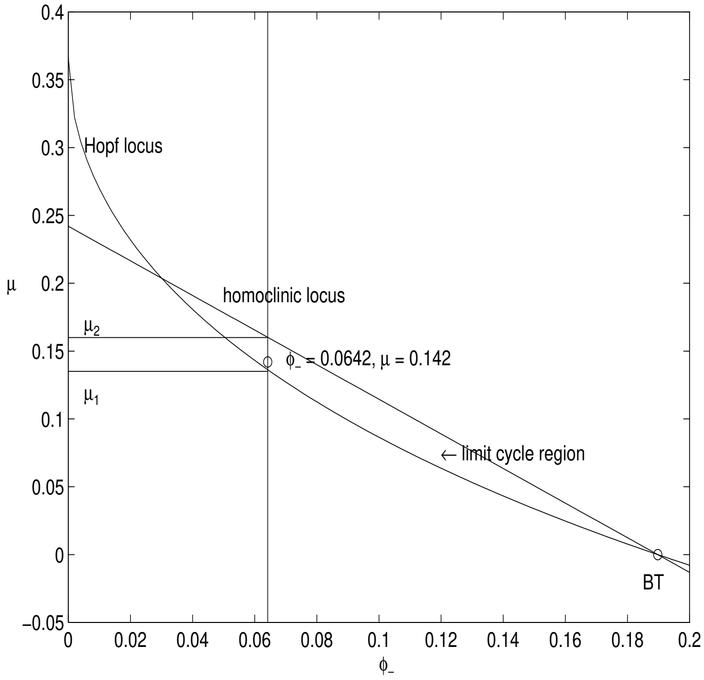

Figure 5: Universal unfolding of the Bogdanov-Takens bifurcation for the shallow water equations. The figure shows the Hopf and the homoclinic bifurcation loci in the unfolding of the Bogdanov-Takens bifurcation calculated for the viscosity parameters $a = 13.0116, b = 5.9114$ and $c = 3.1429$. The Bogdanov-Takens bifurcation, denoted by BT, occurs at the boundary of the Majda-Pego region determined by $\phi_-^* = 0.1897$. The region between the Hopf and the homoclinic locus contains the points for which the corresponding dynamical system has a limit cycle. One such point, $(\phi_-, \mu) = (0.0642, 0.142)$, is shown in this figure. The associated phase space portrait showing the limit cycle is depicted in Figure 1 on the right.

3.1 Shallow Water Equations

The waves that could be used to construct a scale-invariant solution that consists of constant states, rarefaction waves and jump discontinuities are 1- and 2-rarefaction waves, viscous admissible compressive 1 and 2-shock waves, composite waves (adjoint rarefaction waves and shock waves of the same family), viscous admissible transitional shock waves, transitional rarefaction waves, and overcompressive shock waves. It is proved in Ref. [5] that only the classical 1- and 2-rarefaction waves and the classical 1- and 2-shock waves that satisfy the viscous profile entropy criterion occur in the shallow water equations. Therefore, these are the only waves that can be used to construct a Riemann solution. Using wave curve analysis it was shown that a Riemann solution consisting of these waves does not exist for a class of Riemann initial data and an open set of viscosity matrices described below.

The Riemann initial data (U_L, U_R) has the property that there is a limit cycle surrounding one of the critical points, U_L or U_R, in the dynamical system (4) with a fixed viscosity matrix of the form

$$D = \begin{bmatrix} a & -b \\ -b & c \end{bmatrix}, \tag{16}$$

where $ac - b^2 > 0$. Such initial data are obtained by studying the universal unfolding of the Bogdanov-Takens bifurcation that takes place at the boundary of the unstable Majda-Pego region. In our case $a = 13.0116$, $b = 5.9144$ and $c = 3.1429$ and the Majda-Pego region is shown in Figure 4. Our initial data arises in the universal unfolding of the Bogdanov-Taken bifurcation that takes place at the boundary where $\phi_- = \phi_-^* = 0.1897$. The universal unfolding is shown in Figure 4. In this figure the two parameters that determine a dynamical system are ϕ_- and $\mu = s - \lambda_2(U_-)$. Here s is the shock speed and $\lambda_2(U_-)$ is the second eigenvalue of the Jacobian $F'(U)$ evaluated at (v_-, ϕ_-), given by $\lambda_2(U_-) = v_- + \sqrt{\phi_-}$. The values of the parameters (ϕ_-, μ) that determine the dynamical system in which two of the critical points correspond to our initial data (10) are given by $\mu = 0.142$ and $\phi_- = \phi_R = 0.0642$. This point is also shown in Figure 4. It lies in the region between the Hopf and the homoclinic bifurcation loci that contain points for which the associated dynamical system has a limit cycle. The phase space portrait depicting the limit cycle is shown in Figure 1 on the right.

Thus, the initial data we consider in this paper (10) and the viscosity matrix (11) fall into the class studied in Ref. [5]. Theorem 3 from Ref. [5] implies nonexistence of a Riemann solution to this initial-value problem.

3.2 Three-Phase Flow Model

In this section we present the main result of Ref. [3] which states that the Riemann problem for the three-phase flow model described in the previous section, does not have a self-similar weak solution consisting of constant states, rarefaction waves and/or jump discontinuities.

In contrast with the shallow water equations, the model discussed here admits nonclassical shock waves. Namely, it is shown in Ref. [3] that a complete list of waves that may comprise a solution of the Riemann problem (12), (13), (14), (15) is given by the following: 1- and 2- rarefactions waves, 1- and 2-shock waves admitting a viscous profile, 1- and 2-composite waves (adjoint rarefaction waves and shock waves of the same family), and transitional shock waves admitting a viscous profile.

Nonexistence of a self-similar weak solution was established by first considering solutions containing only classical waves, then solutions containing one transitional wave, and finally solutions containing two or more transitional waves. It was shown that none of these cases leads to the existence of a weak solution. In each case a construction breaks down because either the speeds of concatenated waves are not in increasing order, or the admissibility of shocks cannot be established.

4 Main Results

In this section we describe the main results and the method we use to study solutions that arise in the situations, described in Section 3, when a self-similar weak solution of a Riemann problem does not exist.

We study the behavior of solutions of the parabolic system

$$U_t + F(U)_x = \epsilon D U_{xx} \tag{17}$$

with Riemann initial data. We study this behavior numerically by implementing a linearized Crank-Nicholson method, as used by Beam and Warming in [2].

Define $U_1(x,t,\epsilon)$ to be the numerical solution of (17) with Δx and Δt selected for stability, and $U_l(x,t,\epsilon/l)$ to be the numerical solution of

$$U_t + F(U)_x = \frac{\epsilon}{l} D U_{xx}$$

with $\Delta x/l$ and $\Delta t/l$. In the region of strict hyperbolicity, for the data described in Section 3, we find that solutions U_l exhibit continuously generated oscillations. We show that these oscillations are not a characteristic of the numerical method. We prove that in the limit, as $l \to \infty$, the oscillatory solutions U_l converge to the measure-valued solution of the hyperbolic problem.

4.1 Description of the Method

The linearized Crank-Nicholson method, which is a second order implicit finite difference method, can be specified as follows. Let Δx and Δt represent the increments in space and time respectively. Let the solution at a grid point be denoted by U_j^n, where U_j^n approximates the exact solution to (17) at $x = j\Delta x,\ t = n\Delta t$. We define a piecewise constant approximate solution by $U(x,t) \equiv U_j^n$ for all $(x,t) \in [x_j - \Delta x/2, x_j + \Delta x/2) \times [t_n, t_n + \Delta t)$. For each time step the solution of the following block tridiagonal system gives the increments $\delta U_j^n \equiv U_j^{n+1} - U_j^n$.

$$\begin{aligned} \tfrac{1}{\Delta t}\delta U_j^n \quad &+ \quad \tfrac{1}{2\Delta x}\{F(U_{j+1}^n) - F(U_{j-1}^n) + \tfrac{1}{2}F'(U_{j+1}^n)\delta U_{j+1}^n - \tfrac{1}{2}F'(U_{j-1}^n)\delta U_{j-1}^n\} \\ &= \quad \tfrac{1}{(\Delta x)^2}\epsilon D\{U_{j+1}^n - 2U_j^n + U_{j-1}^n + \tfrac{1}{2}[\delta U_{j+1}^n - 2\delta U_j^n + \delta U_{j-1}^n]\}. \end{aligned} \tag{18}$$

The linearization assumption, $F(U_j^{n+1}) \approx F(U_j^n) + F'(U_j^n)\delta U_j^n$, is made to avoid the solution of a nonlinear system at each step.

The following invariance property of this method will prove useful later.

Remark 1 *The numerical method defined by* (18) *is invariant under the transformation* $(\Delta x, \Delta t, \epsilon) \mapsto (\Delta x/k, \Delta t/k, \epsilon/k)$.

Since we are solving Riemann problems, the states U_j^0 with negative j have one value, and the states U_j^0 with nonnegative j have another, regardless of what Δx is, and the fact that our system of equations does not change (except in size) when scaled by k, and that changes in U move with a finite propagation speed, shows that U_j^n with Δx, Δt, and ϵ is equal to U_j^n with $\Delta x/k$, $\Delta t/k$, and ϵ/k.

This method, including the linearization, has a local truncation error, $\tau = \mathcal{O}(\Delta t((\Delta x)^2 + (\Delta t)^2))$. Furthermore, the method is L^∞ linearly stable [24].

4.2 Measure-Valued Solutions

The invariance property of the system shown in Section 4.1 encourages us to define a sequence of numerical solutions in the following manner. Let $U_1(x,t,\epsilon)$ be the solution obtained by solving (17) with Riemann initial data for some $\epsilon > 0$ using the discretization $\Delta x, \Delta t$. Denote by $U_l(x,t,\epsilon_l)$ the solution of (17) with ϵ replaced by $\epsilon_l = \epsilon/l$, i.e.,

$$U_t + F(U)_x = \epsilon_l D U_{xx}, \tag{19}$$

using the discretization $\Delta x/l,\ \Delta t/l$. Then the following invariance property holds.

Proposition 1 *The solution $U_l(x,t,\epsilon_l)$ is equal to $U_1(lx,lt,\epsilon)$.*

Proof: Let $(x,t) \in [(j-\frac{1}{2})\Delta x/l, (j+\frac{1}{2})\Delta x/l) \times [n\Delta t/l, (n+1)\Delta t/l)$ for some integers j and n. So $U_l(x,t,\epsilon_l) = U_{l,j}^n$, the numerical solution of (19) at the grid point (j,n). The point $(lx,lt) \in [(j-\frac{1}{2})\Delta x, (j+\frac{1}{2})\Delta x) \times [n\Delta t, (n+1)\Delta t)$. Thus $U_1(lx,lt,\epsilon) = U_{1,j}^n$. Since $U_{l,j}^n = U_{1,j}^n$ we have $U_l(x,t,\epsilon_l) = U_1(lx,lt,\epsilon)$. ∎

This fact allows the first approximation to serve as the whole sequence. Therefore, instead of reducing epsilon, we push further out in time.

Remark 2 *The sequence U_l is uniformly bounded in L^∞.*

We show this property numerically. Namely, since the viscosity matrix in both examples described in Section 2 is different from a multiple of the identity matrix, the standard theory for proving uniform boundedness based on finding (positively) invariant regions for nonlinear parabolic systems (see [26], [7]) does not apply to these cases. This is why we demonstrate this property numerically. We ran several numerical experiments on both examples described in Section 2. We present the results of one experiment related to the shallow water equations. The same behavior is numerically observed in the three-phase flow solutions. Figures 5 and 6 demonstrate the boundedness of two elements in the sequence. The left figures of 5 and 6 were calculated with $\epsilon = 2.66$, $\Delta x = 9.33$, and $\Delta t = 2.01$. The right figures were calculated with $\epsilon = .133$, $\Delta x = .4667$, and $\Delta t = .1007$. The equations and Riemann initial data are specified in (17), (9), (11) and (10). Notice that as ϵ decreases (ℓ increases) the amplitude of the waves does not increase, only the frequency of the waves does.

This property, together with Lemma 1 implies

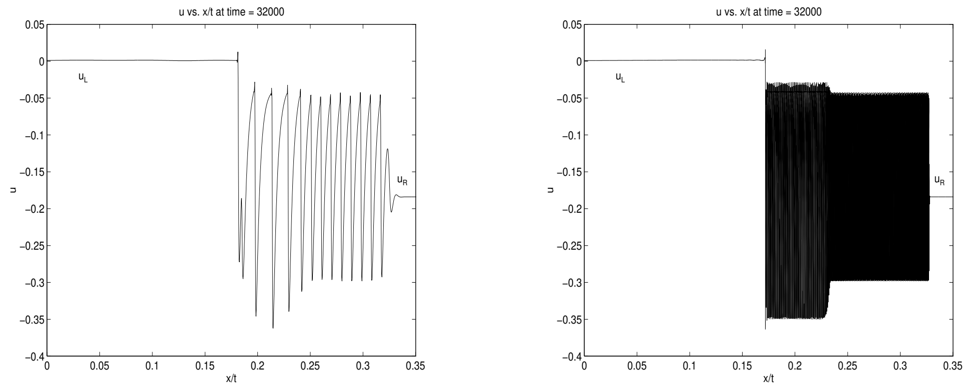

FIGURE 6: Shallow Water Equations: The left picture shows the numerical solution, u, of a parabolic problem with $\epsilon = 2.66$. The right picture shows the numerical solution, u, of the same parabolic problem with $\epsilon = 0.133$.

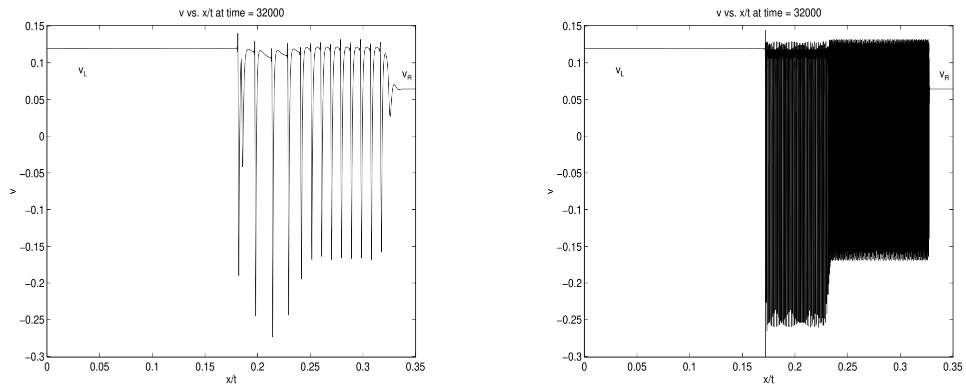

FIGURE 7: Shallow Water Equations: The left picture shows the numerical solution, v, of a parabolic problem with $\epsilon = 2.66$. The right picture shows the numerical solution, v of the same parabolic problem with $\epsilon = 0.133$.

REMARK 3 *There exists a subsequence, U_{l_k}, of U_l, and a measure-valued function $\nu_{x,t}$ such that for all $h \in C(\mathbf{R}^2)$ $h(U_{l_k}(x,t)) \to \overline{h}(x,t)$, in the weak-* topology of L^∞.*

In the following theorem we prove that the limit of a converging subsequence is a measure-valued *solution* of the system of conservation laws. To simplify notation, with a slight abuse of notation, in the rest of the paper we shall denote by U_k the subsequence U_{l_k} of U_l.

THEOREM 1 *If U_k is a converging subsequence of the sequence U_l of solutions of* (19) *defined by the numerical method* (18)*, then the measure-valued function $\nu_{x,t}$ generated by the subsequence U_k is a measure-valued solution to the system of conservation laws.*

Proof: We need to show that the measure-valued function $\nu_{x,t}$ is a solution in the sense of Definition 1. Recall that $U^n_{k,j}$ denotes the discrete approximation to the exact solution of the parabolic problem (19) (with k instead of ℓ) at the point $(x_j, t_n) = (j\Delta x_k, n\Delta t_k)$, where $\Delta x_k = \Delta x/k$, and $\Delta t_k = \Delta t/k$. We introduce the following numerical flux function

$$\begin{aligned}\hat{F}(U^n_k; j) &\equiv \frac{1}{2}[F(U^n_{k,j+1}) + \frac{1}{2}F'(U^n_{k,j+1})(U^{n+1}_{k,j+1} - U^n_{k,j+1}) \\ &+ F(U^n_{k,j}) + \frac{1}{2}F'(U^n_{k,j})(U^{n+1}_{k,j} - U^n_{k,j})].\end{aligned} \tag{20}$$

In terms of $\hat{F}$, the linearized Crank-Nicolson method (18) can be written as

$$\begin{aligned}\frac{1}{\Delta t_k}[U^{n+1}_{k,j} - U^n_{k,j}] &+ \frac{1}{\Delta x_k}[\hat{F}(U^n_k; j) - \hat{F}(U^n_k; j-1)] = \frac{1}{2(\Delta x_k)^2}\epsilon_k D[U^n_{k,j+1} \\ &- 2U^n_{k,j} + U^n_{k,j-1} + U^{n+1}_{k,j+1} - 2U^{n+1}_{k,j} + U^{n+1}_{k,j-1}].\end{aligned} \tag{21}$$

If we multiply though by $\Delta x_k\, \Delta t_k\, \phi(x_j, t_n)$ where $\phi \in C^\infty_0$, sum over all values of n and j, and employ summation by parts we get

$$\begin{aligned}&\Delta x_k \Delta t_k \sum_{n=0}^{\infty}\sum_{j=-\infty}^{\infty} \frac{1}{\Delta t_k}[\phi(x_j, t_n) - \phi(x_j, t_{n-1})]U^n_{k,j} + \\ &\Delta x_k \Delta t_k \sum_{n=0}^{\infty}\sum_{j=-\infty}^{\infty} \frac{1}{\Delta x_k}[\phi(x_{j+1}, t_n) - \phi(x_j, t_n)]\hat{F}(U^n_k; j) =\end{aligned}$$

$$\begin{aligned}\Delta x_k \Delta t_k &\sum_{n=0}^{\infty}\sum_{j=-\infty}^{\infty}[\epsilon_k D\frac{1}{2(\Delta x_k)^2}(\phi(x_{j+1}, t_n) - 2\phi(x_j, t_n) \\ &+ \phi(x_{j-1}, t_n))U^n_{k,j} + \epsilon_k D\frac{1}{2(\Delta x_k)^2}(\phi(x_{j+1}, t_n) - 2\phi(x_j, t_n) \\ &- \phi(x_{j-1}, t_n))U^{n+1}_{k,j}] + \Delta x_k \sum_{j=-\infty}^{\infty}\phi(x_j, 0)U^0_{k,j}.\end{aligned} \tag{22}$$

Due to the compact support of ϕ, all the boundary terms are zero, except the one at $t = 0$. Let $[0, M] \times [-N, N]$ contain the support of ϕ, and let $G = \max_{x,t}\{|D^\alpha\phi|, |\alpha| \leq 3\}$. Taking the limit as $k \to \infty$,*i.e.*, $(\Delta x_k,\ \Delta t_k,\ \epsilon_k) \to (0, 0, 0)$, of equation (22), we consider each pair of sums individually. Starting with the first term, we use a Taylor expansion on ϕ and introduce $\overline{U} \equiv \langle \nu_{x,t}, U\rangle$ to obtain

$$\begin{aligned}&\lim_{k\to\infty}\ \Delta x_k \Delta t_k \sum_{n=0}^{\infty}\sum_{j=-\infty}^{\infty}\frac{1}{\Delta t_k}[\phi(x_j, t_n) - \phi(x_j, t_{n-1})]U^n_{k,j} = \\ &\lim_{k\to\infty}\ \Delta x_k \Delta t_k \sum_{n=0}^{\infty}\sum_{j=-\infty}^{\infty}[\phi_t(x_j, t_n) - \frac{\Delta t_k}{2}\phi_{tt}(x_j, \zeta_n)][\overline{U}(x_j, t_n) + (U^n_{k,j} - \overline{U}(x_j, t_n))]\end{aligned}$$

for $\zeta_n \in (t_{n-1}, t_n)$. Multiplying the two sums in the square brackets gives four terms. The first satisfies

$$\lim_{k\to\infty} \Delta x_k \Delta t_k \sum_{n=0}^{\infty} \sum_{j=-\infty}^{\infty} \phi_t(x_j, t_n)\overline{U}(x_j, t_n) = \int_0^M \int_{-N}^N \overline{U}(x,t)\phi_t(x,t)dxdt.$$

The second converges to zero by the argument,

$$\begin{aligned} &\lim_{k\to\infty} \quad |\Delta x_k \Delta t_k \quad \sum_{n=0}^{\infty} \sum_{j=-\infty}^{\infty} \phi_t(x_j, t_n)(U_{k,j}^n - \overline{U}(x_j, t_n))| \leq \\ &\lim_{k\to\infty} \quad \Delta x_k \Delta t_k \quad G \sum_{n=0}^{\infty} \sum_{j=-\infty}^{\infty} |(U_{k,j}^n - \overline{U}_k(x_j, t_n))| + |R_{\overline{U}_k}(x_j, t_n)|, \end{aligned}$$

where $\overline{U}_k$ is the piecewise constant function defined by $\overline{U}_k(x,t) = \overline{U}(x_j, t_n)$ for all $(x,t) \in [x_j - \Delta x_k/2, x_j + \Delta x_k/2) \times [t_n, t_n + \Delta t_k)$ and $\overline{U}_k(x,t) + R_{\overline{U}_k}(x,t) = \overline{U}(x,t)$. This allows us to replace the first sum with an integral. Also note that since $\overline{U}$ is integrable, $R_{\overline{U}_k}$ goes to zero uniformly as k goes to infinity. We then get

$$\begin{aligned} \lim\nolimits_{k\to\infty} \quad & G\left(\int_0^M \int_{-N}^N |U_k - \overline{U}_k(x,t)|dxdt + \Delta x_k \Delta t_k \sum_{n=0}^{\infty} \sum_{j=-\infty}^{\infty} |R_{\overline{U}_k}(x_j, t_n)| \right) \\ = \quad & \lim_{k\to\infty} G \int_0^M \int_{-N}^N |U_k - \overline{U}_k(x,t)|dxdt \\ \leq \quad & \lim_{k\to\infty} G \int_0^M \int_{-N}^N |U_k - \overline{U}(x,t)| + |R_{\overline{U}_k}(x,t)|dxdt = 0. \end{aligned}$$

The remainder goes to zero because $\overline{U} \in L^1_{loc}$, which is also where $\overline{h}$ for all continuous h resides. The difference term goes to zero because $\overline{U}$ is the weak-* limit of the U_k's. The other two terms in (23) approach zero due to the second Δt_k term and the integrability of $\overline{U}$.

The limit of the part of (22) involving the numerical flux is of the form,

$$\begin{aligned} &\lim_{k\to\infty} \quad \Delta x_k \Delta t_k \quad \sum_{n=0}^{\infty} \sum_{j=-\infty}^{\infty} \frac{1}{\Delta x_k}[\phi(x_{j+1}, t_n) - \phi(x_j, t_n)]\hat{F}(U_k^n; j) = \\ &\lim_{k\to\infty} \quad \Delta x_k \Delta t_k \quad \sum_{n=0}^{\infty} \sum_{j=-\infty}^{\infty} [\phi_x(x_j, t_n) + \frac{\Delta x_k}{2}\phi_{xx}(\zeta_j, t_n)] \\ &\cdot\{\overline{F}(x_j, t_n) + \frac{1}{2}[(F(U_{k,j+1}^n) - \overline{F}(x_j, t_n)) + \frac{1}{2}F'(U_{k,j+1}^n)(U_{k,j+1}^{n+1} - U_{k,j+1}^n) \\ &+ (F(U_{k,j}^n) - \overline{F}(x_j, t_n)) + \frac{1}{2}F'(U_{k,j}^n)(U_{k,j}^{n+1} - U_{k,j}^n)]\}. \end{aligned} \tag{23}$$

All of these terms except $\phi_x(x_j, t_n)\overline{F}(x_j, t_n)$ will approach zero and the limit in (23) is

$$\int_0^M \int_{-N}^N \overline{F}(x,t)\phi_x(x,t)dxdt.$$

The limit of terms of (22) involving ϵ_k is zero and the boundary term of (22) is a simple integral.

Therefore, in the limit as $k \to \infty$, (22) becomes

$$\int_0^\infty \int_{-\infty}^\infty \{\overline{U}(x,t)\phi_t(x,t) + \overline{F}(x,t)\phi_x\}\, dxdt + \int_{-\infty}^\infty U_0(x)\phi(x,0)dx = 0,$$

for all $\phi \in C_0^\infty$. ■

4.3 Expectation Values

We do not compute the measures $\nu_{x,t}$ directly since we need only to be able to calculate the expectation values $\overline{h}$ for continuous functions h. To this end we use the invariance property of our numerical method to prove the following theorem.

Theorem 2 *For each $h \in C(\mathbf{R}^n)$, the expectation values $\langle \nu_{x,t}, h(U)\rangle$, where $\nu_{x,t}$ is the limit of the subsequence $U_k(x,t,\epsilon_k)$, satisfy*

$$\overline{h} \equiv \langle \nu_{x,t}, h(U)\rangle = \lim_{T\to\infty} \frac{2}{T^2}\int_0^T h(U_1(\frac{x}{t}\tau,\tau,\epsilon))\tau d\tau, \tag{24}$$

whenever the limit converges uniformly for almost every $x/t \in \mathbf{R}$.

Proof: We showed before that $U_k(x,t,\epsilon/k) = U_1(kx,kt,\epsilon)$. With the assumption of L^∞ stability, Theorem 1 shows that the subsequence U_k generates a measure-valued solution $\nu_{x,t}$ to our system of conservation laws. Consider a point $(x,t) \in \mathbf{R} \times (0,\infty)$, and let

$$r_0 = \sqrt{x^2+t^2}, \quad \theta_0 = \tan^{-1}(t/x),$$

where the range of $\tan^{-1}$ is $(0,\pi)$. We also denote by $\Delta(r,\theta)$ the infinitesimal sector $|r-r_0| < \Delta r$, $|\theta-\theta_0| < \Delta\theta$, $\Delta r > 0$, and $\Delta\theta > 0$. The area of $\Delta(r,\theta)$ is $m(\Delta(r,\theta)) = 4r_0\Delta r\Delta\theta$.

Given a continuous function $h \in C(\mathbf{R}^m)$, for a.e. $(x,t) \in \mathbf{R}\times(0,\infty)$,

$$\langle \nu_{x,t}, h\rangle = \lim_{\Delta r+\Delta\theta\to 0} \frac{1}{m(\Delta(r,\theta))}\iint_{\Delta(r,\theta)} \langle \nu_{y,\tau}, h\rangle\, dyd\tau. \tag{25}$$

We are interested in $\overline{h}$ only in the distributional sense so we are working with the right hand side of equation (25). If $h \in C(\mathbf{R}^n)$ is such that the limit in (24) converges uniformly for a.e. $x/t \in \mathbf{R}$, we have

$$
\begin{aligned}
& \frac{1}{m(\Delta(r,\theta))} \iint_{\Delta(r,\theta)} \langle \nu_{y,\tau}, h \rangle \, dy d\tau \\
= \; & \frac{1}{m(\Delta(r,\theta))} \lim_{k\to\infty} \iint_{\Delta(r,\theta)} h(U_k(y,\tau,\epsilon/k)) dy d\tau \qquad (26) \\
= \; & \frac{1}{m(\Delta(r,\theta))} \lim_{k\to\infty} \iint_{\Delta(r,\theta)} h(U_1(ky,k\tau,\epsilon)) dy d\tau \\
= \; & \frac{1}{m(\Delta(r,\theta))} \lim_{k\to\infty} \frac{1}{k^2} \iint_{\Delta(kr,\theta)} h(U_1(r,\theta,\epsilon)) r dr d\theta \\
= \; & \lim_{k\to\infty} \frac{1}{4k^2 r_0 \Delta\theta \Delta r} \int_{\theta_0-\Delta\theta}^{\theta_0+\Delta\theta} \int_{k(r_0-\Delta r)}^{k(r_0+\Delta r)} h(U_1(r,\theta,\epsilon)) r dr d\theta \\
= \; & \frac{1}{2\Delta\theta} \int_{\theta_0-\Delta\theta}^{\theta_0+\Delta\theta} \lim_{k\to\infty} \frac{1}{2k^2 r_0 \Delta r} \int_{k(r_0-\Delta r)}^{k(r_0+\Delta r)} h(U_1(r,\theta,\epsilon)) r dr d\theta \\
= \; & \frac{1}{2\Delta\theta} \int_{\theta_0-\Delta\theta}^{\theta_0+\Delta\theta} \frac{1}{2r_0\Delta r} \left\{ \frac{1}{2}(r_0+\Delta r)^2 \lim_{k\to\infty} \frac{2}{k^2(r_0+\Delta r)^2} \int_0^{k(r_0+\Delta r)} h(U_1(r,\theta,\epsilon)) r dr \right.
\end{aligned}
$$

$$
\left. -\frac{1}{2}(r_0-\Delta r)^2 \lim_{k\to\infty} \frac{2}{k^2(r_0-\Delta r)^2} \int_0^{k(r_0-\Delta r)} h(U_1(r,\theta,\epsilon)) r dr \right\} d\theta. \qquad (27)
$$

By the convergence assumption we have that (27) equals

$$
\frac{1}{2\Delta\theta} \int_{\theta_0-\Delta\theta}^{\theta_0+\Delta\theta} \left\{ \lim_{R\to\infty} \frac{2}{R^2} \int_0^R h(U_1(r,\theta,\epsilon)) r dr \right\} d\theta,
$$

which approaches

$$
\lim_{R\to\infty} \frac{2}{R^2} \int_0^R h(U_1(r,\theta_0,\epsilon)) r dr \quad \text{a.e. as } \Delta\theta \to 0.
$$

■

We mention that the proof of Theorem 2 follows closely that of Theorem 2.4 in Ref. [13] which was presented for a different numerical method, solving the inviscid equations, but with a similar invariance property.

The convergence shown in Theorem 2 implies that (26) does not change if the subsequence is replaced with the whole sequence. This means that the *whole* sequence U_ℓ converges to the measure-valued solution $\nu_{x,t}$.

In the numerical simulations the limit (24) is approximated by the sum,

$$
\overline{h}(x/t) \approx \frac{2}{n(n+1)} \sum_{k=1}^{n} k h(U_1(j_k \Delta x, k\Delta\tilde{t})), \; j_k = \lfloor k\Delta\tilde{t} \frac{x}{t} \frac{1}{\Delta x} \rfloor, \qquad (28)
$$

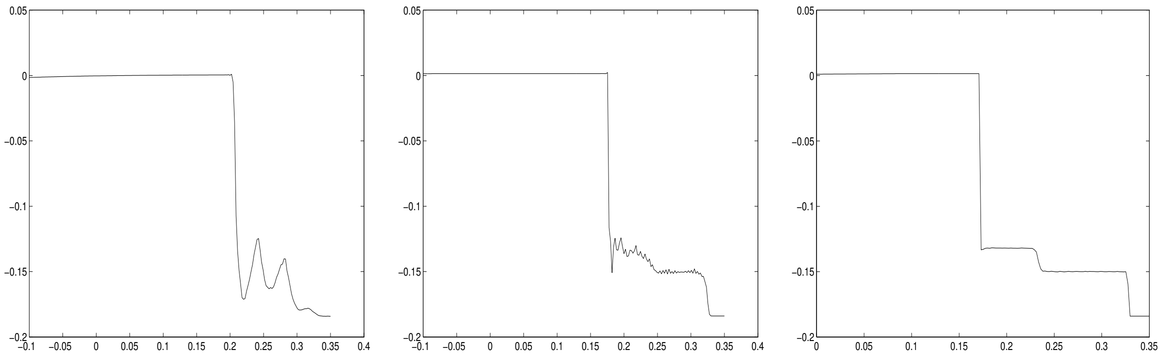

Figure 8: Shallow Water Equations: The figure on the left shows $\bar{u}$ versus x/t using 1/100th of the full partial sum. The figure in the middle shows $\bar{u}$ versus x/t using 1/10th of the full partial sum. The figure on the right shows $\bar{u}$ versus x/t using the full partial sum.

where $\Delta\tilde{t}$ is an increment of t, larger than Δt, such that $T = n\Delta\tilde{t}$. We demonstrate this result on $\overline{u}$, the expectation value of u, the first state space variable, in the shallow water equations. Figure 7 shows graphs of three partial sums made from a numerical solution of the shallow water equations. Figure 7 on the left shows $\bar{u}$ versus x/t using 1/100th of the full partial sum. Figure 7 in the middle shows $\bar{u}$ versus x/t using 1/10th of the full partial sum. Finally, Figure 7 on the right shows $\bar{u}$ versus x/t using the full partial sum. The run that found U_1 to generate these pictures used the Riemann initial data from (10), the matrix given in (11), $\epsilon = .133$, $\Delta x = .4667$, $\Delta t = .1007$, $\tilde{t} = 6.7$, and $T = 32000$. Notice the convergence.

Remark 4 *The expectation values with respect to the underlying Young measure satisfy* $-s\left[\overline{U} - \overline{U}_-\right] + \overline{F}(U) - \overline{F}(U_-) = 0$, *where* $s = x/t$ *is the slope of the line of discontinuity.*

Notice that since F is nonlinear, $\overline{F}(U) \neq F(\overline{U})$ and the system of equations is not closed.

5 Numerical Results

In this section, we present a detailed description of the numerical examples studied in this work. For both the shallow water equations and the three-phase flow model we obtain oscillatory solutions of the parabolic PDE

$$U_t + F(U)_x = \epsilon D U_{xx} \tag{29}$$

that increase in frequency as $\epsilon \to 0$ and stay bounded in amplitude. We calculate expectation values using Theorem 2 and show that they satisfy the system of

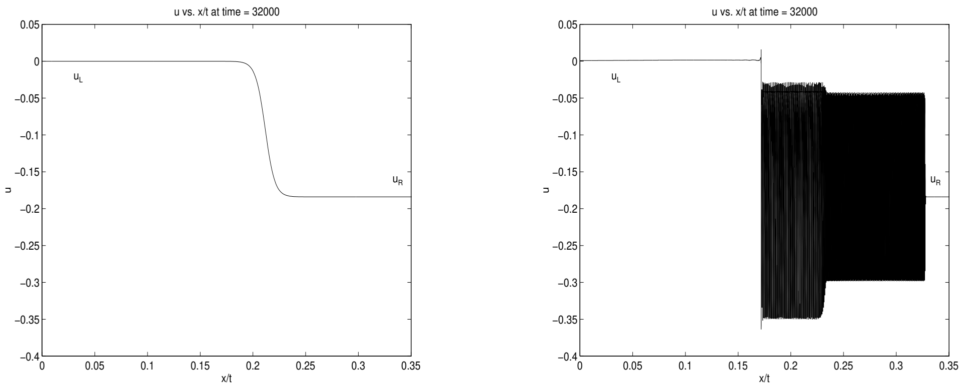

FIGURE 9: Shallow Water Equations: The left picture shows the numerical solution of the parabolic problem for $D = I$. The numerical solution corresponds to a single profilable shock, as predicted by the theory. The right picture shows the oscillations when D is given by (11). The oscillations increase in frequency as $\epsilon \to 0$, but always have uniformly bounded amplitude.

conservation laws in a measure-valued sense. In both examples, the initial data corresponds to a single Lax admissible shock that does not admit a profile due to the presence of a limit cycle. The expectation values with respect to the underlying Young measure consist of more than one shock.

5.1 THE SHALLOW WATER EQUATIONS

We study the parabolic problem (29) for the shallow water equations with F given in (9) and D given by (11). We consider Riemann initial data given by (10). As mentioned in Section 2 this shock initial data corresponds to a Lax 2-shock that does not admit a viscous profile due to a limit cycle surrounding the attractor U_R . The corresponding phase space portrait is shown in Figure 1 on the right. When $D = I$ there exists a connecting orbit in the dynamical system (4) with $U_- = U_L$. The corresponding phase space portrait is shown in Figure 1 on the left. This figure shows a connecting orbit from the saddle point U_L to the attractor U_R.

We solve the parabolic problem with the linearized Crank-Nicolson method. For $D = I$, $\Delta x = 31.11$, $\Delta t = 21.02$, and $\epsilon = 20$, we obtain the expected shock traveling at the correct speed. See the left figure in Figure 8. With D given by (11), $\Delta x = .4667$, $\Delta t = .1007$, and $\epsilon = .133$ we see persistent oscillations. See the right figure in Figure 8. The function U is approximated over the x-interval $[-2000, 12000]$ out to time $T = 32000$. Figure 8 shows u versus x/t for these two cases. For the second case, as time increases, the oscillations increase in frequency over the same x/t intervals. Compare the oscillatory solution u to its expectation values $\overline{u}$ as shown in Figure 9. The expectation values were calculated with equation (28) using $\Delta\tilde{t} = 6.7$ out to time $T = 32000$, updating the sum during the run at each $\Delta\tilde{t}$ increment. The plots of $\overline{v}$ and $\overline{g}$ are similar.

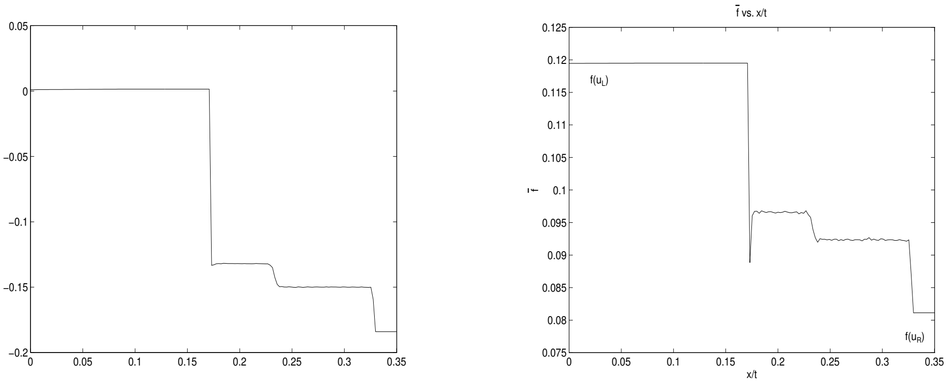

Figure 10: Shallow Water Equations: These figures show the expectation values of u and f obtained for the numerical simulation shown in Figure 8 on the right.

From Theorem 1 and Theorem 2 we know that the expectation values $\overline{U} = (\bar{u}, \bar{v})$ represent a measure-valued solution of the hyperbolic problem. Indeed, we verify that this is the case with our numerical simulations. Namely, we show numerically that the expectation values $\overline{U} = (\overline{u}, \overline{v})$ and $\overline{F} = (\overline{f}, \overline{g})$ satisfy the hyperbolic system of conservation laws in a measure-valued sense. First, we observe that the expectation value of the solution, $\overline{U}$, consists of three shocks. The location of the middle states, $\overline{U}_{M1}$ and $\overline{U}_{M2}$ relative to the oscillations is shown in Figure 10. Each of the shocks travel with a speed s which has to be such that

$$s(\overline{U}_{+} - \overline{U}_{-}) = \overline{F}_{+} - \overline{F}_{-}. \tag{30}$$

Table 1 shows the values of s obtained from $s = (\overline{f}_{+} - \overline{f}_{-})/(\overline{u}_{+} - \overline{u}_{-})$ compared to the numerically observed s.

Table 1: Shallow Water Equations: Rankine-Hugoniot conditions

$\overline{u}_{-}$	$\overline{u}_{+}$	$\overline{f}_{-}$	$\overline{f}_{+}$	s	$(\overline{f}_{+} - \overline{f}_{-})/(\overline{u}_{+} - \overline{u}_{-})$
0.001	-0.132	0.1200	0.0965	0.173	0.177
-0.132	-0.150	0.0965	0.0923	0.236	0.233
-0.150	-0.184	0.0923	0.0811	0.330	0.329

5.2 Three-phase Flow Model

As mentioned before, we study solutions of (29) with the flux function given by (13) with $c = 0.23$, and D given by (14). We consider Riemann initial data given by (15). As described in Section 2, this is shock initial data which corresponds to a Lax admissible 1-shock. However, this shock does not have a viscous profile because of a limit cycle surrounding the repellor U_L in the dynamical system (4). The corresponding phase space portrait is shown in Figure 2. As in the shallow

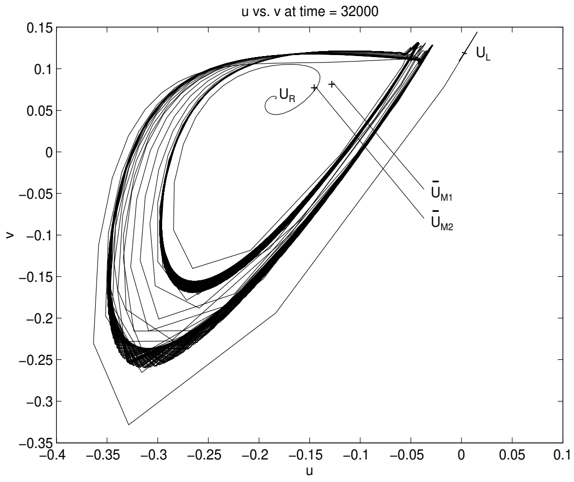

Figure 11: Shallow Water Equations: State space picture, v vs. u, showing oscillations and the expectation values $\overline{U}_{M1}$ and $\overline{U}_{M2}$.

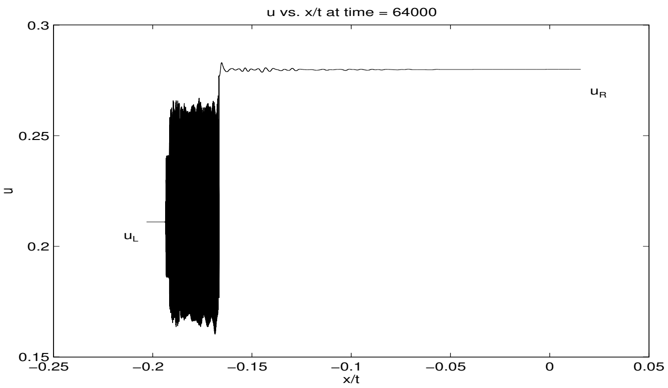

Figure 12: Three-Phase Flow: Oscillations in u when D is given by (14). The frequency of oscillations increases, whereas the amplitude stays uniformly bounded as $\epsilon \to 0$.

water equations, if we let $D = I$, then there is a connecting orbit in state space and the numerical solution consists of the initial shock traveling at a constant speed. However, with D given by (14), $\Delta x = .187$, $\Delta t = .192$, and $\epsilon = .215$ we once again have persistent oscillations. The function U is approximated over the x-interval $[-13000, 1000]$ out to time $T = 64000$. Figure 11 shows u vs. x/t for this case. Again, as time increases, the oscillations increase in frequency over the same x/t interval while maintaining a fixed amplitude. Compare this to the expectation values $\overline{u}$ and $\overline{f}$ in Figure 12. These expectation values were calculated using equation (28) with $\Delta\tilde{t} = 10.0$ out to time $T = 64000$. The plots of $\overline{v}$ and $\overline{g}$ are similar. Just as in the shallow water equations, Theorem 1 and Theorem 2 show that these shocks are weak solutions of the hyperbolic problem.

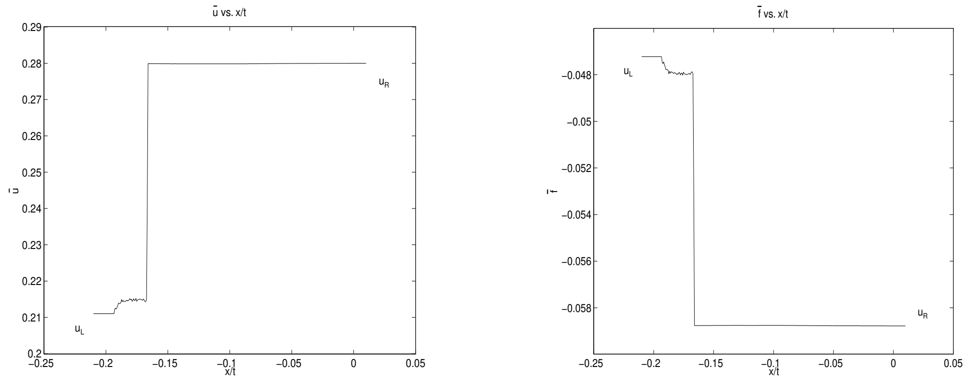

FIGURE 13: Three-Phase Flow: The figures show the expectation values of u and f.

We numerically verified that the Rankine-Hugoniot jump conditions (30) are satisfied by the two shocks in $\overline{U}$ and $\overline{F}$.

6 APPENDIX A

To emphasize the fact that regions containing linearly unstable points in the sense of Majda and Pego, as described in Section 1.1, arise in realistic models and occupy a nontrivial subregion of the state space, we calculated the region of Majda-Pego unstable points for the three-phase flow equations given below, in terms of the saturation variables of each phase, s_i, rather than expanding the model equations about the "center" of the elliptic region to obtain the quadratic model we studied in this paper. One reason for this is to see the size of the "unstable" region relative to the entire state space (defined by $s_i \leq 1, s_1+s_2 \leq 1$). The equations are given by

$$\begin{bmatrix} s_1 \\ s_2 \end{bmatrix}_{\hat{t}} + \begin{bmatrix} \frac{-\lambda_1}{\lambda_1+\lambda_2+\lambda_3} \\ \frac{-\lambda_2}{\lambda_1+\lambda_2+\lambda_3} \end{bmatrix}_x = \left(D \begin{bmatrix} s_1 \\ s_2 \end{bmatrix}_x \right)_x ,$$

where the capillary pressure diffusion matrix is given by

$$D \equiv \begin{bmatrix} \lambda_1(\lambda_3+\lambda_2)\frac{\partial p_{c1}}{\partial x} & -\lambda_1\lambda_2\frac{\partial p_{c2}}{\partial x} \\ -\lambda_1\lambda_2\frac{\partial p_{c1}}{\partial x} & \lambda_2(\lambda_3+\lambda_1)\frac{\partial p_{c2}}{\partial x} \end{bmatrix} \frac{\kappa}{\lambda_1+\lambda_2+\lambda_3}.$$

See Ref. [1]. Here κ is the rock permeability, λ_i is the phase mobility of the i-th phase which is equal to the relative permeability κ_i divided by the corresponding viscosity μ_i, and the capillary pressures are given by

$$\begin{aligned} p_{c1} &\equiv p_1 - p_3 \\ p_{c2} &\equiv p_2 - p_3 \end{aligned}$$

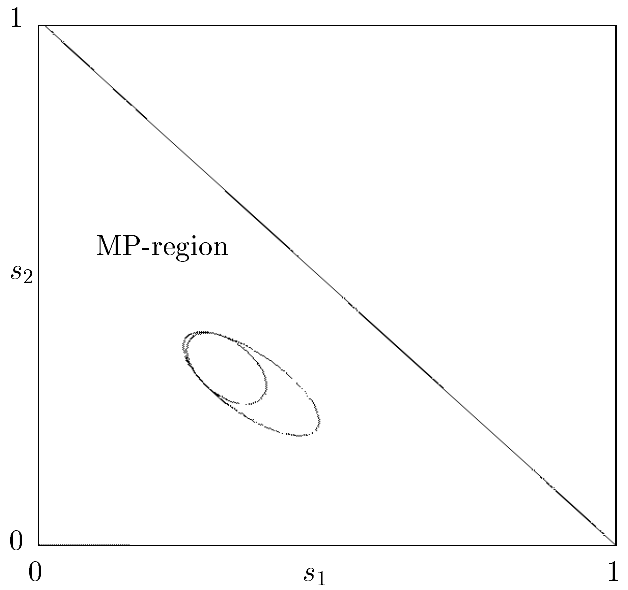

FIGURE 14: A Three-Phase Flow Model: The elliptic region is the interior of the smaller ellipse. The Majda-Pego unstable region is the interior of the larger ellipse (including the elliptic region). The state space is the lower triangle consisting of all the points s_i such that $s_1 + s_2 \leq 1$.

where p_i is the pressure in the ith phase. We assume that $\mu_1 = \mu_2 = \mu_3 = 1$ and that $\kappa_i = s_i^2 + a_i(c, s_1, s_2)$ for $(i = 1, 2, 3)$ with $c = 0.1$. Linearization of the capillary pressure diffusion matrix about a point gives a nontrivial region of Majda-Pego unstable points. Figure 13 shows the MP-unstable region for the linearization about the point $s_1 = 0.4, s_2 = 0.25$. The unstable region is the interior of the outer ellipse.

7 APPENDIX B

To show that the oscillations observed with the Crank-Nicolson method are characteristic of the equations and not of the numerics, we performed two tests. First, we implemented a cubic spline Galerkin method and compared the numerical results with the Crank-Nicolson method and secondly, we compared the runs in both numerical methods with different discretization parameters. See Figure 14.

The cubic splines discretize the PDE (29) in space giving a system of ODE's in time. This system is then solved in time with a second order Runge-Kutta routine. The resulting method has a truncation error of $\mathcal{O}((\Delta x)^4 + (\Delta t)^2)$, which makes it different than the linearized Crank-Nicolson method. This Galerkin method gave the same oscillations when run with identical initial conditions, suggesting that the oscillations are not numerical aberrations.

This is in addition to the fact that, as Δx and Δt are reduced with a fixed ϵ and T, the oscillations are unchanged when using either method. This is illustrated

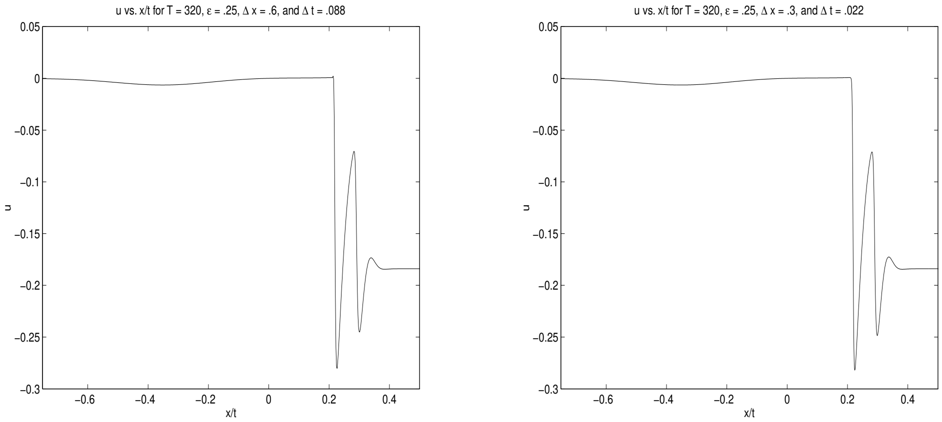

Figure 15: Shallow Water Equations: The left graph is from a run with $\Delta x = .6$ and $\Delta t = .088$. The right graph is from a run with $\Delta x = .3$ and $\Delta t = .022$.

in Figure 14. These graphs show two short runs of the linearized Crank-Nicolson method. Each run used the Riemann initial data from (10), the matrix given in (11), $T = 320$, and $\epsilon = .25$. The data on the left in Figure 14 comes from a run with $\Delta x = .6$ and $\Delta t = .088$. The data on the right in Figure 14 comes from a run with $\Delta x = .3$ and $\Delta t = .022$. Despite the different discretizations the results are indistinguishable and contain oscillations. If the oscillations were numerical then they would depend on the choice of Δx and Δt, which they do not.

Acknowledgements

The authors are grateful to Profs. James Glimm and Bradley Plohr for their valuable suggestions, comments and encouragement.

References

[1] M. B. Allen III, G. A. Behie, and J. A. Trangenstein, "Multiphase Flow in Porous Media: Mechanics, Mathematics, and Numerics," Springer-Verlag, New York, 1988.

[2] R. M. Beam and R. F. Warming, An implicit finite-difference algorithm for hyperbolic systems of conservation laws, *J. Comp. Phys.* **22** (1976), 87–110.

[3] S. Čanić, Nonexistence of Riemann solutions for a quadratic model deriving from petroleum engineering, submitted.

[4] S. Čanić, Quadratic systems of conservation laws with generic behavior at infinity, *J. Dynamics Differential Equations* **9(3)** (1997), 401–426.

[5] S. Čanić and G. R. Peters, Nonexistence of Riemann solutions and Majda-Pego instability, submitted.

[6] S. ČANIĆ AND B. J. PLOHR, Shock wave admissibility for quadratic conservation laws, *J. Differential Equations* **118** (1995), 293–335.

[7] K. N. CHUEH, C. CONLEY, AND J. A. SMOLLER, Positively invariant regions for systems of nonlinear diffusion equations, *Indiana University Math. J.* **26** (1997), 372–411.

[8] C. C. CONLEY AND J. A. SMOLLER, Viscosity matrices for two-dimensional nonlinear hyperbolic systems, *Comm. Pure Appl. Math.* **23** (1970), 867–884.

[9] R. J. DIPERNA, Measure-valued solution to conservation laws, *Arch. Rational Mech. Anal.* **88** (1985), 223–270.

[10] R. J. DIPERNA AND A. MAJDA, Oscillations and concentrations in weak solutions of the incompressible fluid equations, *Comm. Math. Phys.* **108** (1987), 667–689.

[11] L. FOY, Stady-state solutions of hyperbolic systems of conservation laws with viscosity terms, *Comm. Pure Appl. Math.* **17** (1964), 177–188.

[12] H. FRID, Measure-valued solution for multiphase flow in porous media: existence and weak asymptotic steadiness of waterflooding, *Matematica Contemporanea* **8** (1995), 177–201.

[13] H. FRID AND I.-S. LIU, Oscillation waves in Riemann problems inside elliptic regions for systems of mixed type, *ZAMP* **46** (1995), 913–931.

[14] H. FRID AND I.-S. LIU, Oscillation waves in Riemann problems for phase transitions, *Quart. J. Appl. Math.* **56** (1998), 115–135.

[15] F. FURTADO, Structural stability of nonlinear waves for conservation laws, Ph. D. thesis, New York University, New York, 1989.

[16] I. M. GEL'FAND, Some problems in theory of quasilinear equations, *Trans. Amer. Math. Soc.* **29** (1963), 295–381.

[17] E. ISAACSON, D. MARCHESIN, B. PLOHR, AT AL., Riemann problem solver package, *http://ftp.ams.sunysb.edu/pub/rp/*.

[18] E. L. ISAACSON, D. MARCHESIN, AND B. PLOHR, Transitional waves for conservation laws, *SIAM J. Math. Anal.* **21** (1990), 837–866.

[19] P. D. LAX, Hyperbolic systems of conservation laws, II, *Comm. Pure Appl. Math.* **X** (1957), 537–566.

[20] P. D. LAX, The entropy condition and the admissibility of shocks, *J. Math. Anal. Applications* **240** (1976), 78–88.

[21] R. J. LEVEQUE, "Numerical Methods in Conservation Laws," Lecture Notes in Mathematics, Birkhäuser Verlag, Berlin 1992.

[22] A. Majda and R. Pego, Stable viscosity matrices for systems of conservation laws, *J. Differential Equations* **56** (1985), 229–133.

[23] M. S. Mock, A topological degree for orbits connecting critical points of autonomous systems, *J. Differential Equations* **38** (1980), 176–191.

[24] G. R. Peters, Oscillatory solutions in conservation laws related to nonexistence of weak self-similar solutions, Ph. D. thesis, Iowa State University, Ames, 1997.

[25] D. G. Schaeffer and M. Shearer, The classification of 2×2 systems of non-strictly hyperbolic conservation laws, with application to oil recovery, *Comm. Pure Appl. Math.* **XL** (1987), 141–178.

[26] J. A. Smoller, "Shock Waves and Reaction-Diffusion Equations," Springer-Verlag, New York, 1983.

[27] L. Tartar, Compensated compactness and applications to partial differential equations, *in* "Research Notes in Mathematics, Nonlinear Analysis and Mechanics **4**," (R. J. Knops, Ed.), 136–212, Pitman Press, New York, 1979.

[28] K. Zumbrun, A third look at the anomalous shocks of Conley and Smoller, private communication.